TẠP CHÍ KHOA HỌC
TRƯỜNG ĐẠI HỌC QUY NHƠN

Nghiên cứu cơ chế và động học phản ứng giữa methylene blue với gốc tự do OH trong pha khí bằng phương pháp tính toán DFT

Lưu Thị Thu Thảo[1,2], Trần Thanh Hiền[1], Nguyễn Thị Thủy[1], Nguyễn Minh Thông[1], Võ Văn Quân[3,*]

[1]Trường Đại học Sư phạm, Đại học Đà Nẵng, Việt Nam
[2]Trung tâm Giáo dục Quốc tế IEC, Quảng Ngãi, Việt Nam
[3]Trường Đại học Sư phạm Kỹ thuật, Đại học Đà Nẵng, Việt Nam

Ngày nhận bài: 13/07/2025; Ngày sửa bài: 01/11/2025;
Ngày nhận đăng: 11/11/2025; Ngày xuất bản: 28/02/2026

TÓM TẮT

Methylene blue (**MB**) là một loại thuốc nhuộm dị vòng thơm phổ biến, được sử dụng rộng rãi trong công nghiệp, đặc biệt là trong nhuộm giấy, bông, len, lụa và các loại sợi dệt khác. Cơ chế và động học liên quan đến quá trình phân hủy **MB** bởi gốc tự do HO• trong pha khí đã được tính toán trong nghiên cứu này bằng phương pháp hóa học lượng tử. Trong pha khí, **MB** chủ yếu bị phân hủy thông qua cơ chế cộng gốc tự do vào nối đôi, trong đó gốc HO• tấn công tại vị trí C4 ở nhiệt độ 298,15 K. Hằng số tốc độ tổng thể của bước 1 và bước 2 lần lượt là $3{,}24\times10^{10}$ $M^{-1}\,s^{-1}$ và $1{,}48\times10^{12}$ $M^{-1}\,s^{-1}$; quá trình này tạo ra ba sản phẩm chính gồm . Hằng số tốc độ tổng thể của phản ứng phân hủy **MB** có xu hướng giảm nhẹ ($k_{overall} = 6.63 \times 10^{10} - 1.81 \times 10^{10}$ $M^{-1}\,s^{-1}$) trong khoảng nhiệt độ từ 253 đến 323 K.

Từ khóa: *Methylene blue, tính toán DFT, oxidation, cơ chế, phân hủy.*

**Tác giả liên hệ chính.*
Email: vvquan@ute.udn.vn

QUY NHON UNIVERSITY
JOURNAL OF SCIENCE

DFT Study on the mechanism and kinetics of the gas-phase reaction between methylene blue and OH radicals

Luu Thi Thu Thao[1,2], Tran Thanh Hien[1], Nguyen Thi Thuy[1], Nguyen Minh Thong[1], Quan V. Vo[3,*]

[1]The University of Danang - University of Sciences and Education, Vietnam
[2]IEC International Education Center, Quang Ngai, Vietnam
[3]The University of Danang - University of Technology and Education, Vietnam

Received: 13/07/2025; Revised: 01/11/2025;
Accepted: 11/11/2025; Published: 28/02/2026

ABSTRACT

Methylene blue (**MB**) is a representative aromatic heterocyclic dye extensively employed in industrial applications, particularly in the dyeing of paper, cotton, wool, silk, and related textiles. In this work, the mechanisms and kinetics governing the gas-phase degradation of MB by hydroxyl radicals (HO•) were elucidated through quantum chemical calculations. The results demonstrated that, at 298.15 K, **MB** predominantly underwent degradation *via* a radical adduct formation mechanism involving HO• addition at the C4 position. The overall rate constants for the first and second steps were calculated to be 3.24×10^{10} and 1.48×10^{12} M^{-1} s^{-1}, respectively, leading to three major products. The overall degradation rate exhibited only a slight variation with increasing temperature from 253 to 323 K, suggesting that temperature exerts a limited effect on the oxidative removal efficiency of MB under environmentally relevant conditions.

Keyworks: *Methylene blue, DFT study, oxidation, mechanism, chemical fate.*

1. INTRODUCTION

Methylene blue (**MB**, Figure 1) is an aromatic heterocyclic dye widely utilized in industry, particularly for dyeing silk, cotton, wool, paper, and other materials.[1-3] **MB** is a cationic dye that is resistant to natural degradation, posing a risk to ecological systems and potentially leading to different health problems for humans in the event of uncontrolled release, despite its recognized clinical use.[2-6] **MB** degradation can be significantly promoted by various oxidation technologies, such as electrochemical,[7] photocatalytic[8-10] and ozone[11] process. Among advanced oxidation processes (AOPs), the introduction of reactive oxygen species - ROS (including HO•, $SO_4^{\bullet-}$, Cl•, ClO•, HOO•, and $O_2^{\bullet-}$), represents a simple yet highly effective approach. Notably, the HO• was regarded as the primary oxidizing species responsible for **MB** degradation due to its high redox potential and non-selective reactivity.[12,13] Our recent analysis revealed that, in water, **MB** exhibited a quick reaction with the HO• radical, characterized by an overall rate constant ranging from 5.51×10^9 to 2.38×10^{10} M^{-1} s^{-1}, and a lifetime of 11.66 hours to 5.76 years at temperatures between 273 and 383 K.[14]

**Corresponding author.*
Email: vvquan@ute.udn.vn

https://doi.org/10.52111/qnjs.2026.20112

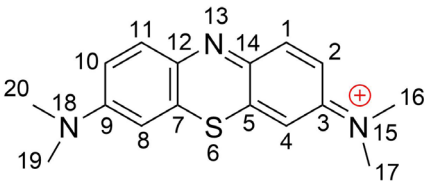

Methylene blue (MB)

Figure 1. Structure of **MB**.

Given that **MB** can persist in aerosol drying layers, dye particulates, and spray processes,[15,16] where solvent influences are substantially reduced, elucidating its gas-phase degradation mechanism offers valuable complementary insights into its atmospheric transformation behavior. Nonetheless, the atmospheric degradation of **MB** has yet to be investigated. This study examines the thermodynamic and kinetic aspects of the reaction between **MB** and hydroxyl radicals in the gas phase through computational methods.

2. COMPUTATIONAL METHODS

Computational calculations for this investigation were performed using the Gaussian 16 software suite at the M06-2X/6-311++G(d,p) level of theory.[17] This methodology is widely recognized for its precision in determining thermodynamic and kinetic properties in modern computational chemistry studies.[18-20] Kinetic evaluations were conducted using the Quantum Mechanics-based Overall Free Radical Scavenging Activity (QM-ORSA) approach.[21] This method has proven to yield reliable results, showing minimal errors from experimental observations (k_{calc}/k_{exp} = 1−2.9),[21-23] and has been extensively applied in kinetic investigations of radical reactions.[14,24,25] Under standard conditions of 1 M concentration and temperatures ranging from 253 to 323 K in the gas phase,[26] the reaction rate constant (k) was computed employing equation (1) and transition state theory (TST).[27-33]

$$k = \sigma\kappa \frac{k_B T}{h} e^{-(\Delta G^{\neq})/RT} \quad (1)$$

The Gibbs free energy of activation, denoted as $\Delta G^{\ddagger}$, is used in conjunction with the Boltzmann constant (k_B) and the Planck constant (h). Tunneling corrections (κ) were calculated based on the Eckart barrier model.[34] The reaction symmetry number is represented by σ. [35,36]

The radical adduct formation **(**RAF), or formal hydrogen transfer (FHT) pathways of the **MB** + HO reaction were detailed in processes (2-3):[20,32,37]

RAF: **MB-H** + HO$^{\bullet}$ → [**HO-MB-H**]$^{\bullet}$ (2)

FHT: **MB-H** + HO$^{\bullet}$ → **MB**$^{\bullet}$ + H_2O (3)

3. RESULTS AND DISCUSSION

3.1. Topology optimization of MB

MB can exist in multiple conformers; therefore, all possible conformations were systematically screened,[38] and the conformer exhibiting the lowest electronic energy was selected for subsequent analysis. The topology optimization was conducted to elucidate the molecular geometry and identify the most stable conformer. The M06-2X/6-311++G(d,p) level of theory was employed to optimize the molecular structure and to investigate the thermodynamic and kinetic characteristics of the degradation of MB by HO$^{\bullet}$ radicals. The optimized structural parameters of MB are summarized in Table 1, and the corresponding optimized geometry is illustrated in Figure S1 (Supporting Information).

Table 1. Bond lengths (Å) and bond angles (°) in **MB**.

Bond	Length	Bond	Length	Bond	Angle
C5−S	1.735	C7−S	1.735	C5SC7	103.4
C12−N13	1.328	C14−N13	1.328	C12−N13−C14	123.8
C3−N15	1.342	C2−C3	1.439	C2−C3−N15	120.6
C16−N15	1.462	C17−N15	1.460	C16−N15−C17	119.0
C9−N18	1.342	C9−C10	1,439	C10−C9N18	120,6

Bond	Length	Bond	Length	Bond	Angle
C1−C2	1.356	C2−C3	1.439	C1−C2−C3	120.6
C3−C4	1.417	C4−C5	1.379	C3−C4−C5	120.6
C5−C14	1.434	C4−C5	1.379	C4−C5−C14	121.4
C5−C14	1.434	C1−C14	1.429	C1−C14−C5	117.0
C10−C11	1.356	C11−C12	1.430	C10−C11−C12	122.1
C11−C12	1.430	C12−C7	1.434	C11−C12−C7	121.4
C7−C8	1.379	C8−C9	1.417	C7−C8−C9	120.6

Table 1 illustrates that the C5–S bond length is equal to the C7–S bond length (1.735 Å), and these atoms form a bond angle of 103.4°. The C12–N13 bond length and C14–N13 are also equal, measured at 1.328 Å, with a corresponding bond angle of 123.8°. The bond lengths of C1–C2 (1.356 Å) and C4–C5 (1.379 Å) are shorter than those of C2–C3 (1.439 Å), C3–C4 (1.417 Å), and C5–C14 (1.434 Å). The bond angles C1–C2–C3 and C3–C4–C5 show only negligible differences (120.6°). Compared with the experimental crystal structure of **MB**,[39] the calculated bond lengths and bond angles exhibit no significant deviations. Therefore, the optimized structure of **MB** is in good agreement with the experimental structure and is thus suitable for subsequent computational analyses.

3.2. The reaction of MB with HO• in the atmospheric environment

3.2.1. Thermodynamic evaluation

Table 2. Gibbs free energy change (ΔG°, kcal/mol) of the reaction between **MB** and HO• via different mechanisms in the gas phase at 298.15 K.

Mechanism	Position	ΔG°
FHT	C16−H	−30.0
	C17−H	−30.1
RAF	N13	−11.1
	C1	−15.4
	C2	−17.9
	C3	−4.4
	C4	−16.1
	C5	−11.7
	C14	−11.6

To assess the reactivity of **MB** at various carbon and nitrogen atomic sites via different reaction mechanisms, the Gibbs free energy change (ΔG°, kcal/mol) was evaluated. The results are summarized in Table 2.

A positive ΔG° value indicates that a reaction is thermodynamically unfavorable and non-spontaneous, whereas a negative ΔG° value corresponds to a thermodynamically favorable and spontaneous process. As presented in Table 2, the calculated ΔG° values reveal that both the FHT and RAF mechanisms proceed spontaneously. In particular, the RAF mechanism exhibits negative ΔG° values at the C1, C2, C3, C4, C5, N13, and C14 positions, while the FHT mechanism shows negative ΔG° values at the C16 and C17 positions. The ΔG° values for these reactive sites range from −4.4 to 30.1 kcal/mol, suggesting thermodynamically favorable pathways for these reactions. Consequently, the subsequent kinetic investigation focuses on the thermodynamically favorable reactions (ΔG° < 0) proceeding through the FHT and RAF mechanisms.

3.2.2. Kinetic evaluation

The kinetics of the **MB** + HO• reaction were comuputed following the QM-ORSA protocol.[21] The results are summarized in Table 3 and the representative transition state structures are illustrated in Figure 2. As shown in Table 3, the reaction between **MB** and HO• radicals in the gas phase proceeds rapidly, with an overall rate constant of 3.24×10^{10} M^{-1} s^{-1} for the first step. The degradation of MB was defined by the FHT mechanism at the C16 and C17 positions and by the RAF mechanism at the C2 and C4 positions.

https://doi.org/10.52111/qnjs.2026.20112

The calculated rate constants at these reactive sites decrease in the following order: C4 (2.65×10^{10} $M^{-1}s^{-1}$) > C17 (3.01×10^{9} $M^{-1}s^{-1}$) > C16 (1.51×10^{9} $M^{-1}s^{-1}$) > C2 (1.39×10^{9} $M^{-1}s^{-1}$). Accordingly, the relative abundances of the corresponding intermediates follow the order: **GI4** (81.7%) > **GI17** (9.3%) > **GI16** (4.6%) > **GI2** (4.3%).

These computational results suggest that the first step reaction preferentially proceeds via the RAF mechanism, rather than through the FHT mechanism. The intermediate originating from C4 contributes most significantly (81.7%) compared to the other three positions. This dominance can be attributed to the higher electron density at C4 relative to C2, making C4 more favorable for HO• radical addition. Within the FHT pathway, the reaction is more favorable at C17 (9.3%) than at C16 (4.6%), likely due to the lower bond dissociation energy of the C17−H bond compared with C16−H.

In the second step, reactions involving transition states **GI2, GI4, GI16** and **GI17,** indicate that degradation predominantly proceeds through the **GI4** intermediate. The **GI4** predominantly undergoes degradation via the **RAF** mechanism. The most favorable site is C14, exhibiting a rate constant of 9.84×10^{11} $M^{-1}s^{-1}$ and leading to the formation of product **GP3**, which accounts for 66.5% of the total product yield. This is followed by C2, with a rate constant of 3.89×10^{11} $M^{-1}s^{-1}$, resulting in product **GP1** at 26.3%.

Table 3. Gibbs free energy of activation $\Delta G^{\ddagger}$ (kcal/mol), tunneling corrections κ, rate constants (k_{Eck}, k_r, $k_{overall}$ $M^{-1}s^{-1}$), and branching ratio Γ (%) of the HO + **MB** reaction.

Comp.	Mechanisms	Positions	$\Delta G^{\ddagger}$	κ	k_{Eck}	*r*	k_r	Γ	Products
MB	FHT	C16−H	6.0	2.0	1.51×10^{9}			4.6	**GI16**
		C17−H	5.5	1.9	3.01×10^{9}			9.3	**GI17**
	RAF	C1	10.1	1.4	7.23×10^{9}			0.0	
		C2	5.5	1.2	1.39×10^{9}			4.3	**GI2**
		C3	10.9	1.2	1.45×10^{5}			0.0	
		C4	3.7	1.1	2.65×10^{10}			81.7	**GI4**
		C5	12.7	1.3	7.83×10^{3}			0.0	
		N13	13.1	1.6	4.94×10^{3}			0.0	
		C14	8.2	1.3	1.51×10^{7}			0.0	
	$k_{overall}$(**MB** + HO•, step 1)				**3.24×10^{10}**				
GI4	FHT	C16−H	7.1	6.8	8.43×10^{8}	0.817	6.89×10^{8}	0.0	
		C17H	9.5	2.5	5.24×10^{6}	0.817	4.28×10^{6}	0.0	
		C19−H	6.0	1.7	1.26×10^{9}	0.817	1.03×10^{9}	0.1	
		C20−H	6.2	1.8	9.64×10^{8}	0.817	7.87×10^{8}	0.1	
	RAF	C1	8.2	1.3	7.83×10^{6}	0.817	6.40×10^{6}	0.0	
		C2	1.6	1.1	4.76×10^{11}	0.817	3.89×10^{11}	26.3	**GP1**
		C3	3.8	1.2	$1.26\times1^{01}0$	0.817	1.03×10^{10}	0.7	
		C5	6.9	1.5	8.43×10^{7}	0.817	6.89×10^{7}	0.0	
		C7	11.9	1.3	1.63×10^{4}	0.817	1.33×10^{4}	0.0	
		C8	2.6	1.1	8.43×10^{10}	0.817	6.89×10^{10}	4.7	**GP2**
		C9	13.5	1.2	1.02×10^{3}	0.817	8.37×10^{2}	0.0	

Comp.	Mechanisms	Positions	ΔG‡	κ	k_{Eck}	*r*	k_r	Γ	Products
		C10	7.7	1.3	1.69×10^{7}	0.817	1.38×10^{7}	0.0	
		C11	10.9	1.3	7.83×10^{4}	0.817	6.40×10^{4}	0.0	
		C12	11.8	1.4	1.93×10^{4}	0.817	1.57×10^{4}	0.0	
		C14	1.0	1.0	1.20×10^{12}	0.817	9.84×10^{11}	**66.5**	**GP3**
		N13	15.0	1.7	1.08×10^{2}	0.817	88.60	0.0	
	$k_{overall}$ (r) (**GI4** + HO•)						1.45×10^{12}	98.3	
$k_{overall}$ (*r*) (**MB** + HO•, step 2)							1.48×10^{12}		

At the C8 position, the reaction proceeds with a rate constant of 6.89×10^{10} M^{-1} s^{-1}, yielding product **GP2** with a contribution of 4.7%. C3 position has a rate constant of 1.03×10^{10} M^{-1} s^{-1}, generating only 0.7% of the product. Reactions via the **FHT** mechanism also occur at **C19** and **C20** positions, but their contributions are minimal (0.1% each). Therefore, the main products of the second step are **GP1**, **GP2**, and **GP3**, corresponding to the **C2, C8,** and **C14** positions of the **GI4** transition state.

Based on the above analysis, it can be concluded that in the gas phase at 298.15 K, **MB** is primarily degraded by the HO• radical via the RAF mechanism at the C4 position, leading to the formation of three major products (**GP1, GP2**, and **GP3)**. The overall rate constants for steps 1 and 2 are 3.24×10^{10} M^{-1} s^{-1} and 1.48×10^{12} M^{-1} s^{-1}, respectively.

Compared with the reaction of **MB** with HO• radicals in the aqueous phase,[14] the results indicate that the first-step reaction proceeds rapidly in both the gas phase and water, with overall rate constants of 3.24×10^{10} and 1.02×0^{10} M^{-1} s^{-1}, respectively. However, the second-step reaction in the gas phase ($k_{overall}$ = 1.48×10^{12} M^{-1} s^{-1}) is faster than that in water, with ($k_{overall}$ = 9.39×10^{9} M^{1} s^{-1}). Furthermore, distinct mechanistic pathways and product distributions were observed in the two environments, highlighting the significant role of the surrounding medium in modulating the reaction energetics and kinetics of HO•-induced **MB** degradation.

3.2.3. Effect of temperature on the degradation of MB in the gas phase

To investigate the effect of temperature on the degradation of **MB**, the rate constants for reactions at various positions of **MB** were calculated within the typical environmental temperature range (253−323 K, equivalent to -20°C to 50°C). The results are presented in Figure 3. As the gas-phase temperature increases, all rate constants associated with the **FHT** mechanism (k16, k17) decrease. In contrast, the rate constants corresponding to the **RAF** mechanism exhibit inconsistent trends: k1, k5, and k14 increase with temperature, while k2 and k4 decrease. Notably, k3 and k13 fluctuate irregularly. In the temperature range of 253 - 323 K, the overall rate constant for **MB** degradation tends to decrease slightly, primarily due to the decline in k16, k17, k2, and k4, which correspond to the four reactive positions previously discussed in Table 3. The study revealed that the decrease in rate constants at the C2, C4, C16, and C17 positions was attributed to the rapid decline of the tunneling corrections (κ) with increasing temperature, from 2.7 to 1.1 in the corresponding reactions. According to the Eyring analysis, this non-Arrhenius behavior arises from a combination of negative activation entropy ($\Delta S^{‡} < 0$), reflecting a highly ordered transition state and the diminished contribution of quantum tunneling at higher temperatures. Similar entropic and tunneling effects have been extensively reported in radical–molecule association reactions, supporting the physical

https://doi.org/10.52111/qnjs.2026.20112

plausibility of the observed trend.[40,41] Among all, k4 is the highest at every temperature (ranging from 6.63×10^{10} M^{-1} s^{-1} to 1.81×10^{10} M^{-1} s^{-1}), indicating that the **RAF** mechanism at the C4 position is the most favorable. Therefore, the primary degradation products of **MB** are those formed via radical addition of HO• to **MB**, specifically **GP1, GP2**, and **GP3**.

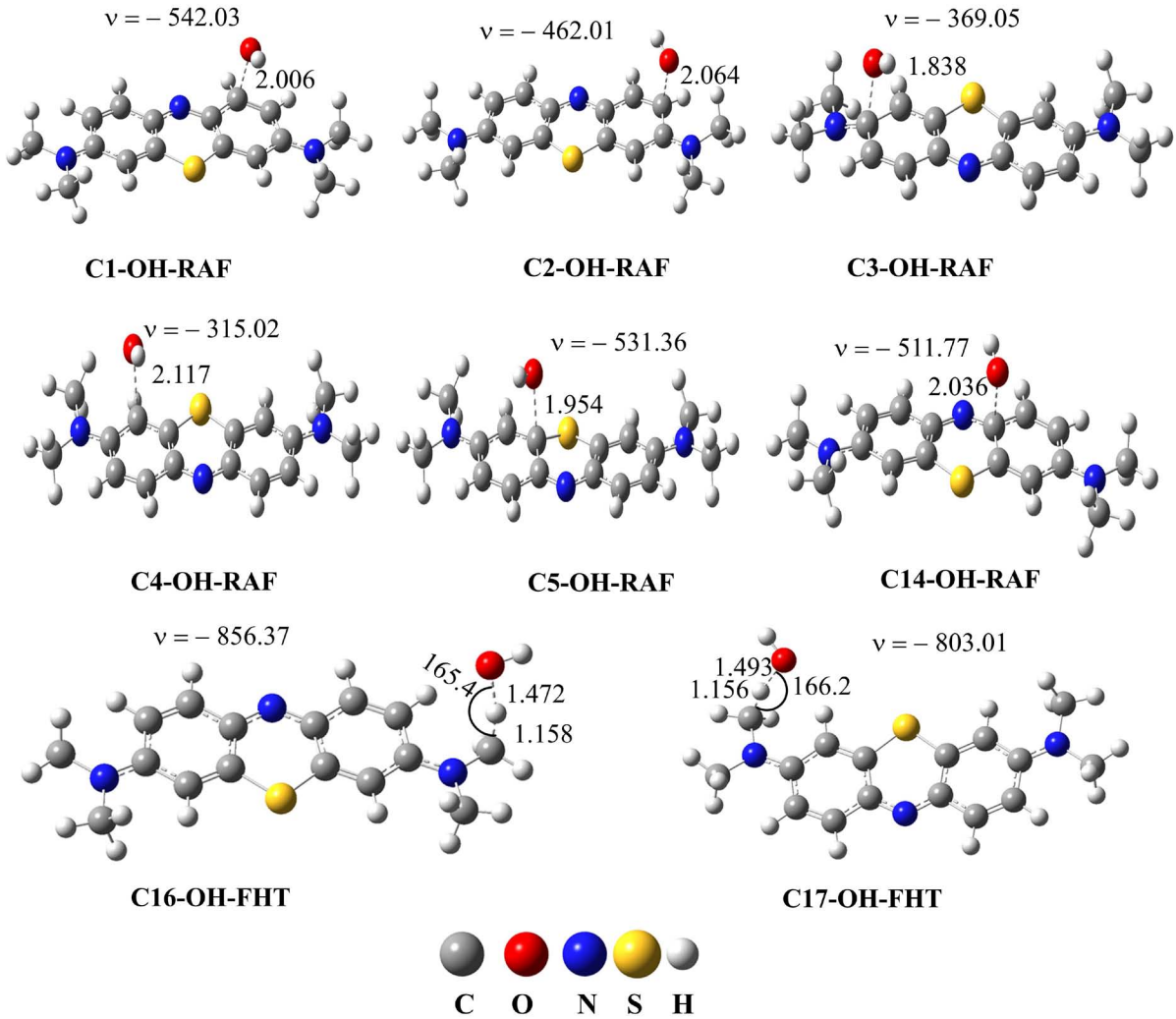

Figure 2. Structures of representative transition states *via* FHT and RAF nechanisms in the gas phase. Bond lengths (Å) and bond angles (°).

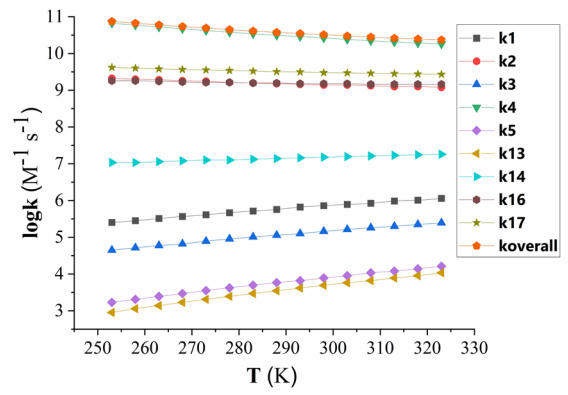

Figure 3. Temperature dependence of rate constants (log *k*) in the gas phase in the range of 253 - 323 K.

4. CONCLUSION

This study elucidated the mechanism and kinetics of **MB** degradation HO• radicals in the gas phase using quantum chemical calculations. At 298.15 K, MB degradation primarily proceeded via the **RAF** reaction occurring at the C4 position. This pathway led to the formation of three major products (**GP1**, **GP2**, and **GP3**), with the overall rate constants for the first and second reaction steps determined to be 3.24×10^{10} $M^{-1}s^{-1}$ and 1.48×10^{12} $M^{-1}s^{-1}$, respectively. Within the temperature range of 253–323 K, variations

in the rate constants of individual reactive sites were observed; however, the **RAF** at the C4 position consistently dominated the **MB** + HO• degradation process. Consequently, the overall degradation rate exhibited a minor decrease ($k_{overall}$ = 6.63×10^{10}−1.81×10^{10} M^{-1} s^{-1}).

Acknowledgments

This research is funded by the Vietnamese Ministry of Education and Training under project number B2024.DNA.09.

REFERENCES

1. M. I. Din, R. Khalid, J. Najeeb, Z. Hussain. Fundamentals and photocatalysis of methylene blue dye using various nanocatalytic assemblies-a critical review, *Journal of Cleaner Production,* **2021**, *298*, 126567.
2. M. Rafatullah, O. Sulaiman, R. Hashim, A. Ahmad. Adsorption of methylene blue on low-cost adsorbents: a review, *Journal of Hazardous Materials,* **2010**, *177*, 70-80.
3. M. Mohammed, A. Shitu, A. Ibrahim. Removal of methylene blue using low cost adsorbent: a review, *Research Journal of Chemical Sciences,* **2014**, *2231*, 606X.
4. M. Alomar, A. A. Khan, M. Yar. DFT investigation of Co/Ni decorated borophene for efficient removal of methylene blue from wastewater effluent, *Journal of Molecular Liquids,* **2025**, *417*, 126627.
5. I. Ullah, R. B. Neder, M. I. Khan, I. U. Din, H. Parwaz, S. Sufian. Ligand-capped pristine and doped ZnO2 nanoparticles for enhanced photocatalytic methylene blue degradation: a DFT-supported study, *Ceramics International,* **2025**, *51*, 17061-17078.
6. G. Nandhini, D. Vignesh, M. Shobana, T. Pazhanivel, S. Kavita, P. Balaji. Graphene-decorated magnetic cobalt ferrite for effective UV-accelerated photocatalytic degradation of methylene blue: experimental and theoretical insights by DFT, *Emergent Materials,* **2025**, *8*, 29-44.
7. M. Panizza, A. Barbucci, R. Ricotti, G. Cerisola. Electrochemical degradation of methylene blue, *Separation and Purification Technology,* **2007**, *54*, 382-387.
8. F. Banat, S. A. Asheh, M. m. A. Rawashdeh, M. Nusair. Photodegradation of methylene blue dye by the UV/H2O2 and UV/acetone oxidation processes, *Desalination,* **2005**, *181*, 225-232.
9. R. M. Mohamed, I. A. Mkhalid, E. S. Baeissa, M. A. A. Rayyani. Photocatalytic degradation of methylene blue by Fe/ZnO/SiO_2 nanoparticles under visiblelight, *Journal of Nanotechnology,* **2012**, *2012*, 1-5.
10. R. S. Dariani, A. Esmaeili, A. Mortezaali, S. Dehghanpour. Photocatalytic reaction and degradation of methylene blue on TiO_2 nano-sized particles, *Optik,* **2016**, *127*, 7143-7154.
11. J. Zhang, K. H. Lee, L. Cui, T. s. Jeong. Degradation of methylene blue in aqueous solution by ozone-based processes, *Journal of Industrial and Engineering Chemistry,* **2009**, *15*, 185-189.
12. Z. Wang, H. Zhao, H. Qi, X. Liu, Y. Liu. Free radical behaviours during methylene blue degradation in the Fe(2+)/H(2)O(2) system, *Environmental Technology,* **2019**, *40*, 1138-1145.
13. R. H. Waghchaure, V. A. Adole, B. S. Jagdale. Photocatalytic degradation of methylene blue, rhodamine B, methyl orange and Eriochrome black T dyes by modified ZnO nanocatalysts: A concise review, *Inorganic Chemistry Communications,* **2022**, *143*, 109764.
14. Q. V. Vo, L. T. T. Thao, T. D. Manh, M. Van Bay, B. T. T. Le, N. T. Hoa, A. Mechler. Reaction of methylene blue with OH radicals in the aqueous environment: mechanism, kinetics, products and risk assessment, *RSC Advances,* **2024**, *14*, 27265-27273.
15. S. Becagli, C. Ghedini, S. Peeters, A. Rottiers, R. Traversi, R. Udisti, M. Chiari, A. Jalba, S. Despiau, U. Dayan. MBAS (Methylene Blue Active Substances) and LAS (Linear Alkylbenzene Sulphonates) in Mediterranean coastal aerosols: sources and transport processes, *Atmospheric Environment,* **2011**, *45*, 6788-6801.

16. M. Radke. Sterols and anionic surfactants in urban aerosol: emissions from wastewater treatment plants in relation to background concentrations, *Environmental Science & Technology,* **2005**, *39*, 4391-4397.

17. M. J. Frisch, G. W. Trucks, H. B. Schlegel et al. *Gaussian 16/Gaussian, 2016.*

18. M. C. Gonzalez, A. V. Bunge, J. R. A. Idaboy. Thiophenols, promising scavengers of peroxyl radicals: mechanisms and kinetics, *Journal of Computational Chemistry,* **2019**, *40*(24), 2103-2110.

19. N. M. Diez, J. R. A. Idaboy, R. J. Boyd. A quantum chemical and TST study of the OH hydrogen-abstraction reaction from substituted aldehydes: FCHO and ClCHO, *Journal of Physical Chemistry A,* **2001**, *105*, 9034-9039.

20. A. Galano, J. R. A. Idaboy. Kinetics of radical-molecule reactions in aqueous solution: a benchmark study of the performance of density functional methods, *Journal of Computational Chemistry* **2014**, *35*, 2019-2026.

21. A. Galano, J. R. A. Idaboy. A computational methodology for accurate predictions of rate constants in solution: application to the assessment of primary antioxidant activity, *Journal of Computer Chemistry,* **2013**, *34*(28), 2430-2445.

22. J. R. l. A. Idaboy, A. Galano. On the chemical repair of DNA radicals by glutathione: hydrogen vs electron transfer, *Journal of Physical Chemistry B,* **2012**, *116*, 9316-9325.

23. M. E. Alberto, N. Russo, A. Grand, A. Galano. A physicochemical examination of the free radical scavenging activity of Trolox: mechanism, kinetics and influence of the environment, *Physical Chemistry Chemical Physics,* **2013**, *15*, 4642-4650.

24. Q. V. Vo, T. L. B. Tram, N. T. Hoa, A. N. A. Duong, A. Mechler. Hydroxyl radical-initialized polymerization and degradation of N-vinylpyrrolidone in lipid and aqueous environments, *Polymer Degradation and Stability ,* **2023**, *216*, 110483.

25. A. Galano, J. R. A. Idaboy. Computational strategies for predicting free radical scavengers' protection against oxidative stress: where are we and what might follow?, *International Journal of Quantum Chemistry,* **2019**, *119*, e25665.

26. S. M. Papalexiou, A. AghaKouchak, K. E. Trenberth, E. F. Georgiou. Global, regional, and megacity trends in the highest temperature of the year: diagnostics and evidence for accelerating trends, *Earth's Future,* **2018**, *6*, 71-79.

27. M. G. Evans, M. Polany. Some applications of the transition state method to the calculation of reaction velocities, especially in solution, *Transactions of the Faraday Society* **1935**, *31*, 875-894.

28. H. Eyring. The Activated Complex in Chemical Reactions, *The Journal of Chemical Physics,* **1935**, *3*, 107-115.

29. D. G. Truhlar, W. L. Hase, J. T. Hynes. Current status of transition-state Theory, *Journal of Physical Chemistry,* **1983**, *87*, 2664-2682.

30. T. Furuncuoglu, I. Ugur, I. Degirmenci, V. Aviyente. Role of chain transfer agents in free radical polymerization kinetics, *Macromolecules,* **2010**, *43*, 1823-1835.

31. E. Vélez, J. Quijano, R. Notario, E. Pabón, J. Murillo, J. Leal, E. Zapata, G. Alarcón. A computational study of stereospecifity in the thermal elimination reaction of menthyl benzoate in the gas phase, *Journal of Physical Organic Chemistry,* **2009**, *22*, 971-977.

32. E. Dzib, J. L. Cabellos, F. O. Chi, S. Pan, A. Galano, G. Merino. Eyringpy: a program for computing rate constants in the gas phase and in solution, *International Journal of Quantum Chemistry,* **2019**, *119*, e25686.

33. E. Dzib, J. L. Cabellos, F. O. Chi, S. Pan, A. Galano, G. Merino. *Eyringpy 1.0.2,* 2018.

34. C. Eckart. The penetration of a potential barrier by electrons, *Physical Review,* **1930**, *35*, 1303-1309.

35. E. Pollak, P. Pechukas. Symmetry numbers, not statistical factors, should be used in absolute rate theory and in Broensted relations, *Journal of the American Chemical Society,* **1978**, *100*, 2984-2991.

36. A. F. Ramos, B. A. Ellingson, R. M. Pañeda, J. M. Marques, D. G. Truhlar. Symmetry numbers and chemical reaction rates, *Theoretical Chemistry accounts,* **2007**, *118*, 813-826.

37. A. Galano, G. Mazzone, R. A. Diduk, T. Marino, J. R. A. Idaboy, N. Russo. Food antioxidants: chemical insights at the molecular level, *Annual Review of Food Science and Technology,* **2016**, *7*, 335-352.

38. W. Hehre, J. Yu, P. Klunzinger, L. Lou. *Spartan Software*, 2000.

39. H. E. Marr, J. M. Stewart, M. Chiu. The crystal structure of methylene blue pentahydrate, *Acta Crystallographica Section B: Structural Crystallography and Crystal Chemistry,* **1973**, *29*, 847-853.

40. Z. Safaei, A. Shiroudi, E. Zahedi, M. Sillanpaa. Atmospheric oxidation reactions of imidazole initiated by hydroxyl radicals: kinetics and mechanism of reactions and atmospheric implications, *Physical Chemistry Chemical Physics,* **2019**, *21*, 8445-8456.

41. F. Xiao, X. Sun, Z. Li, X. Li. Theoretical study of radical-molecule reactions with negative activation energies in combustion: hydroxyl radical addition to alkenes, *ACS Omega,* **2020**, *5*, 12777-12788.